Fabrication and characterization of high Q polymer micro-ring resonator and its application as a sensitive ultrasonic detector

Tao Ling, Sung-Liang Chen, and L. Jay Guo*

Department of Electrical Engineering and Computer Science, University of Michigan, Ann Arbor, Michigan 48109, USA
**guo@eecs.umich.edu*

Abstract: Smooth sidewall silicon micro-ring molds have been fabricated using resist reflow and thermal oxidation method. High Q factor polymer micro-ring resonators have been fabricated using these molds. Quality factors as high as 10^5 have been measured at telecommunication wavelength range. By carefully examining the different loss mechanisms in polymer micro-ring, we find that the surface scattering loss can be as low as 0.23 dB/cm, much smaller than the absorption loss of the polystyrene polymer used in our devices. When used as an ultrasound detector such a high Q polymer micro-ring device can achieve an acoustic sensitivity around 36.3 mV/kPa with 240 μW operating power. A noise equivalent pressure (NEP) is around 88 Pa over a bandwidth range of 1–75 MHz. We have improved the NEP by a factor of 3 compared to our previous best result.

OCIS codes: (140.4780) Optical resonators; (230.5750) Resonators; (170.7170) Ultrasound; (130.6010) Sensors.

References and links

1. S. Srinivasan, H. S. Baldwin, O. Aristizabal, L. Kwee, M. Labow, M. Artman, and D. H. Turnbull, "Noninvasive, in utero imaging of mouse embryonic heart development with 40-MHz echocardiography," Circulation **98**(9), 912–918 (1998).
2. H. F. Zhang, K. Maslov, G. Stoica, and L. V. Wang, "Functional photoacoustic microscopy for high-resolution and noninvasive *in vivo* imaging," Nat. Biotechnol. **24**(7), 848–851 (2006).
3. H. Nakano, Y. Matsuda, and S. Nagai, "Ultrasound detection by using a confocal Fabry-Perot interferometer with phase-modulated light," Ultrasonic **37**(3), 257–259 (1999).
4. S. Ashkenazi, Y. Hou, T. Buma, and M. O'Donnell, "Optoacoustic imaging using thin polymer etalon," Appl. Phys. Lett. **86**(13), 134102 (2005).
5. P. C. Beard, and T. N. Mills, "Miniature optical fibre ultrasonic hydrophone using a Fabry-Perot polymer film interferometer," Electron. Lett. **33**(9), 801–803 (1997).
6. E. Z. Zhang, and P. Beard, "Ultra high sensitivity, wideband Fabry Perot ultrasound sensors as an alternative to piezoelectric PVDF transducers for biomedical photoacoustic detection," Proc. SPIE **5320**, 222–229 (2004).
7. M. Cai, O. Painter, K. J. Vahala, and P. C. Sercel, "Fiber-coupled microsphere laser," Opt. Lett. **25**(19), 1430–1432 (2001).
8. F. Vollmer, D. Braun, A. Libchaber, M. Khoshsima, I. Teraoka, and S. Arnold, "Protein detection by optical shift of a resonant microcavity," Appl. Phys. Lett. **80**(21), 4057–4069 (2002).
9. M. Borselli, K. Srinivasan, P. E. Barclay, and O. Painter, "Rayleigh scattering, mode coupling, and optical loss in silicon microdisks," Appl. Phys. Lett. **85**(17), 3693–3695 (2004).
10. T. J. Kippenberg, S. M. Spillane, D. K. Armani, and K. J. Vahala, "Fabrication and coupling to planar high-Q silica disk microcavities," Appl. Phys. Lett. **83**(4), 797–799 (2003).
11. A. Gondarenko, J. S. Levy, and M. Lipson, "High confinement micron-scale silicon nitride high Q ring resonator," Opt. Express **17**(14), 11366–11370 (2009), http://www.opticsinfobase.org/abstract.cfm?uri=oe-17-14-11366.
12. P. Rabiei, W. H. Steier, Cheng Zhang, and L. R. Dalton, "Polymer micro-ring filters and modulators," J. Lightwave Technol. **20**(11), 1968–1975 (2002).
13. C. Y. Chao, and L. J. Guo, "Biochemical sensors based on polymer microrings with sharp asymmetrical resonances," Appl. Phys. Lett. **83**(8), 527–529 (2003).

#137270 - $15.00 USD Received 27 Oct 2010; revised 18 Dec 2010; accepted 23 Dec 2010; published 6 Jan 2011

14. H. S. Sun, A. T. Chen, B. C. Olbricht, J. A. Davies, P. A. Sullivan, Y. Liao, and L. R. Dalton, "Direct electron beam writing of electro-optic polymer microring resonators," Opt. Express **16**(9), 6592–6599 (2008), http://www.opticsinfobase.org/oe/abstract.cfm?uri=oe-16-9-6592.
15. I. M. White, H. Oveys, and X. D. Fan, "Liquid-core optical ring-resonator sensors," Opt. Lett. **31**(9), 1319–1321 (2006).
16. T. Ling, and L. J. Guo, "A unique resonance mode observed in a prism-coupled micro-tube resonator sensor with superior index sensitivity," Opt. Express **15**(25), 17424–17432 (2007), http://www.opticsinfobase.org/abstract.cfm?uri=oe-15-25-17424.
17. S. W. Huang, S. L. Chen, T. Ling, A. Maxwell, M. O'Donnell, L. J. Guo, and S. Ashkenazi, "Low-noise wideband ultrasound detection using polymer microring resonators," Appl. Phys. Lett. **92**(19), 193509 (2008).
18. D. K. Armani, T. J. Kippenberg, S. M. Spillane, and K. J. Vahala, "Ultra-high-Q toroid microcavity on a chip," Nature **421**(6926), 925–928 (2003).
19. D. H. Kim, J. G. Im, S. S. Lee, S. W. Ahn, and K. D. Lee, "Polymeric microring resonator using nanoimprint technique based on a stamp incorporating a smoothing buffer layer," IEEE Photon. Technol. Lett. **17**(11), 2352–2354 (2005).
20. C. Y. Chao, and L. J. Guo, "Polymer Micro-ring Resonators Fabricated by Nanoimprint Technique," J. Vac. Sci. Technol. B **20**(6), 2862–2866 (2002).
21. K. K. Lee, D. R. Lim, L. C. Kimerling, J. Shin, and F. Cerrina, "Fabrication of ultralow-loss Si/SiO_2) waveguides by roughness reduction," Opt. Lett. **26**(23), 1888–1890 (2001).
22. H. C. Liu, Y. H. Lin, and W. Hsu, "Sidewall roughness control in advanced silicon etch process," Microsyst. Technol. **10**(1), 29–34 (2003).
23. C. Y. Chao, and L. J. Guo, "Reduction of Surface Scattering Loss in Polymer Microrings Using Thermal-Reflow Technique," IEEE Photon. Technol. Lett. **16**(6), 1498–1500 (2004).
24. K. J. Vahala, *Optical Microcavities* (World Scientific 2004), Chapter 7.
25. M. Oxborrow, "How to simulate the whispering gallery modes of dielectric microresonator in FEMLAB/COMSOL," Proc. SPIE **6452**, 64520J, 64520J-12 (2007).
26. R. K. Chang, and A. J. Campillo, *Optical Processes in Microcavities* (World scientific 1996), Chapter 6.
27. V. R. Almeida, and M. Lipson, "Optical bistability on a silicon chip," Opt. Lett. **29**(20), 2387–2389 (2004).
28. M. Borselli, T. J. Johnson, and O. Painter, "Beyond the Rayleigh scattering limit in high-Q silicon microdisks: theory and experiment," Opt. Express **13**(5), 1515–1530 (2005), http://www.opticsinfobase.org/oe/abstract.cfm?URI=OPEX-13-5-1515.
29. R. G. Hunsperger, *Integrated Optics: Theory and Technology* (Springer Science and Business Media 2009), Chapter 5.
30. J. R. Schwesyg, T. Beckmann, A. S. Zimmermann, K. Buse, and D. Haertle, "Fabrication and characterization of whispering-gallery-mode resonators made of polymers," Opt. Express **17**(4), 2573–2578 (2009), http://www.opticsinfobase.org/oe/abstract.cfm?uri=oe-17-4-2573.

1. Introduction

Ultrasound-related imaging has been widely used in biomedical applications. For example, high-frequency pulsed-echo can non-invasively image mice in very early embryonic stages [1]. Photo-acoustic (PA) microscopy is able to provide the information of total hemoglobin concentration in humans [2]. In these studies, a detector with low noise and wide bandwidth plays an important role in obtaining good imaging quality, especially for *in vivo* PA imaging where a low laser energy is required for safety reasons [2].

Recently, an optical cavity based ultrasound detection platform has attracted increasing interest [3–6,17]. Compared with conventional piezoelectric transducers, the new detection platform provides several advantages, such as preserving high sensitivity with reduced element sizes, high-frequency and wideband response with simple fabrication. In this new optical cavity based detection platform, optically transparent polymer material was used because of its high optical elastic coefficient and high deformability, which can provide a sensitive response under acoustic pressure. A polymer based fiber tip Fabry-Perot (F-P) cavity ultrasonic hydrophone has been demonstrated with comparable sensitivity and noise equivalent pressure (NEP) to current piezoelectric PVDF ultrasonic sensing devices [5]. An improved sensitivity has been realized in a polymer based plane F-P device by increasing the device's Q factor, which results from an increased reflection of the multi-layer stacks based 1-dimension photonic crystal mirror based on multi-layer stacks [6]. Additional improvement of the sensitivity can be achieved by further increasing the reflectivity of the 1-D photonic crystal mirror, but this requires a sophisticated system to precisely control the thickness and uniformity of the deposited multilayer film. Except for the photonic crystal based light confining mechanism, the total internal reflection (TIR) mechanism has been widely used to confine the light in the cavity to achieve a much higher Q factor. High Q resonators using the

#137270 - $15.00 USD Received 27 Oct 2010; revised 18 Dec 2010; accepted 23 Dec 2010; published 6 Jan 2011

TIR mechanism include micro-spheres [7,8], micro-disks [9,10], micro-rings [11–14] and micro-tubes [15,16]. By combining a polymer material's high optical elastic coefficient and high deformability with the TIR-based high Q factor micro-resonators, we have previously demonstrated wideband ultrasound detection with a NEP 20 times better than the best piezoelectric transducer of similar size and bandwidth by using polymer micro-ring devices with a Q of around 6000 [17].

Ultrasound detectors with improved sensitivity can directly benefit ultrasound and PA imaging by allowing imaging at increased depth. Smaller micro-rings have larger angular sensitivity, enabling higher spatial resolution in imaging applications such as beam-forming and PA tomography. Higher sensitivity can be obtained by using the micro-ring resonator with a higher Q factor, which normally requires a ring waveguide with smooth sidewalls to minimize the surface roughness induced scattering loss. Smooth sidewalls are even more important for small size micro-ring devices due to increased scattering loss as compared to large size micro-ring devices. To achieve a smooth sidewall in waveguides, several methods have been used. A thermal reflow method has been used to fabricate ultra-high Q micro-toroids [18], but the cavity size can shrink by tens of microns during the reflow process which makes it very difficult to fabricate the on chip integrated waveguides coupled to such high Q micro-cavities. A smooth buffer layer modified stamp [19] has been used to fabricate an embedded polymer race-track micro-ring with a Q factor as high as 10^5; however, it would be challenging to apply this to micro-rings with small diameters because a very narrow gap from the bus waveguide of few hundred nanometers is required for efficient coupling.

We have previously developed a nano-imprint based technique to fabricate the polymer micro-ring resonators [20]. To significantly improve the resonator's Q factor, we show a new fabrication process in this paper that includes two important steps to reduce the sidewall roughness of the silicon mold for imprinting the micro-ring devices: resist thermal reflow process and thermal oxidation followed with buffered hydrofluoric acid etching process [21]. High Q and smooth sidewall polymer micro-rings can be mass duplicated with such molds by straightforward nano-imprint process. Resonant mode quality factors as high as 10^5 were measured in a polymer micro-ring with a 45 μm radius (R), which corresponds to an optical loss of 1.8 dB/cm. Surface scattering loss, which is normally the dominating term in total loss, was found to be as low as 0.23 dB/cm. Owing to this high Q polymer micro-ring, we have achieved ultrasound detection sensitivity of 36.3 mV/kPa at 240 μW operating power. The device's NEP, which represents the minimum detectable pressures, is 51, 74, and 88 Pa for 1–25, 1–50 and 1–75 MHz bandwidth range, respectively. This is nearly 3 fold lower as compared to our previous best result, making it the most sensitive ultrasound detector of a similar size.

2. Device fabrication and measurement technique

In order to fabricate high Q factor polymer micro-rings using nano-imprint technique, a mold with smooth sidewalls is needed. Many materials such as glass, polymer, metal, and silicon have been examined for mold applications. Among these materials, silicon is the most attractive material candidate due to the excellent processibility of silicon and a wide range of fabrication processes developed by the integrated circuit (IC) industry. In particular dry etching of silicon has been shown to achieve smooth and vertical sidewalls [22], which is ideal for our application. Our silicon mold is fabricated using electron beam lithography followed by reactive ion etch (RIE). Two important modifications are used to further smooth the silicon mold sidewalls. The process starts with a silicon wafer with an initial 400 nm thermal oxide layer. Electron beam lithography is used to create a pattern with a micro-ring and a straight bus waveguide on an 800 nm thick positive electron-beam resist (950k PMMA). The patterns are then transferred to the silicon oxide layer using RIE with PMMA as the etch mask. After this step the PMMA mask is removed in hot acetone. The micro-ring pattern is further transferred onto the silicon wafer by deep silicon etching with the silicon oxide layer as etch mask. After deep silicon etching, the silicon oxide masking layer is removed by buffered hydrofluoric acid (BHF), which completes the master mold fabrication. Two

#137270 - $15.00 USD Received 27 Oct 2010; revised 18 Dec 2010; accepted 23 Dec 2010; published 6 Jan 2011

important steps have been added to this silicon mold fabrication process to achieve smooth sidewalls.

The first important step is the PMMA resist reflow, which is applied before the silicon oxide etch step. By choosing a suitable temperature and time duration, this reflow process can greatly reduce imperfections in the PMMA resist patterns and harden the edge of the PMMA resist. Too low of a temperature will not cause the resist to reflow, while too high of a temperature will cause deformation in the coupling gap region, which could significantly increase the optical loss. After a number of experiments, the appropriate PMMA resist reflowing temperature and time duration was determined to be 115°C for 90 seconds. Figure 1 show the SEM pictures of the imprinted polystyrene micro-ring waveguide sidewalls by using the silicon molds with (1b) and without (1a) the PMMA resist reflow process. We can clearly see from Fig. 1(a) that there is a great amount of roughness on the sidewall of the polymer micro-ring, which is thought to be due to the damage caused by RIE on the edge of the PMMA pattern during etching of SiO2, which eventually gets transferred onto the silicon mold. However, in Fig. 1(b), the sidewall of the polymer micro-ring fabricated from the mold with the PMMA reflowing process has relatively small vertical roughness, which means that the edges of the PMMA are well protected during the RIE process. The spectrum characterization of these two devices will be shown in Section 3.

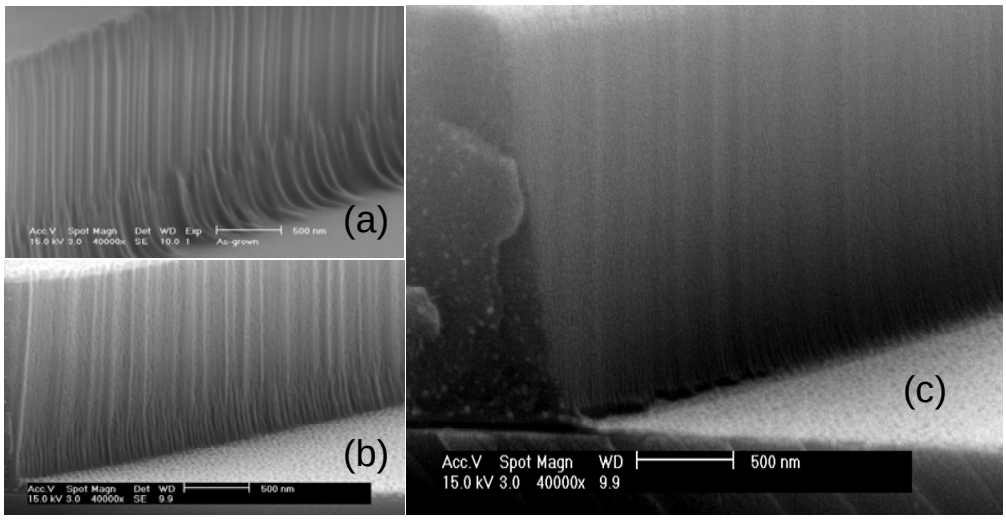

Fig. 1. Sidewall SEM image of the polymer micro-ring fabricated from the mold: (a) without resist reflow process, (b) with resist reflow process, (c) with resist reflow and thermal oxidation process.

The second important step is the thermal oxidation followed by the BHF etching step, which was used to smooth out the roughness after deep silicon etching. The oxidation step is performed in a high temperature furnace that grows around 100 nm of thermal oxide on the silicon surface. During the oxidation process the amount of Si consumed is 44% of final oxide thickness, the rough Si surface layer is converted to SiO2 in this step and removed by BHF etching after the oxidation step. Figure 1(c) shows the sidewall of the imprinted polymer micro-ring using the silicon mold after the thermal oxidation and BHF etching step. We see a major improvement in the sidewall roughness compared to Fig. 1(b). Most of the sharp ripple-like roughness and small holes on the sidewall seen in Fig. 1b have disappeared in Fig. 1(c).

After fabrication, the polymer micro-ring transmission spectra were characterized using a tunable laser (Santec TSL-220) with a wavelength range of 1530-1610nm. The laser's line-width is much smaller than the resonance peak line-width of the polymer micro-ring. The input light polarization was controlled by a fiber based optical polarization controller. In order to make our measurements consistent, we fixed the input light as TE polarization.

#137270 - $15.00 USD Received 27 Oct 2010; revised 18 Dec 2010; accepted 23 Dec 2010; published 6 Jan 2011

3. Polymer micro-ring's loss characterization

The Q factors of waveguide-coupled micro-rings can be classified as two components: $Q_{intrinsic}$ and Q_{couple}, where the former is the Q of an isolated resonator and the latter takes into account of the coupling loss to the bus waveguide. $Q_{intrinsic}$ is primarily limited by the optical losses in an isolated resonator, and can be attributed to these loss mechanisms: radiation loss, surface scattering loss, material absorption loss. Therefore the micro-resonator's overall Q factor can be expressed as:

$$\frac{1}{Q_{total}} = \frac{1}{Q_{\text{int}rinsic}} + \frac{1}{Q_{couple}} = \frac{1}{Q_{rad}} + \frac{1}{Q_{scatt}} + \frac{1}{Q_{abs}} + \frac{1}{Q_{couple}}, \tag{1}$$

where Q_{rad}, Q_{scatt}, and Q_{abs} are radiation loss-related Q, surface scattering loss-related Q, and absorption loss-related Q, respectively. The total loss-related Q and coupling related Q can be extracted from the fitted transmission spectrum [23], the radiation related Q can be obtained from the simulation, the absorption loss-related Q can be measured from a thermal bi-stability effect (will be described in more detail below), and finally the scattering related Q can be extracted from Eq. (1).

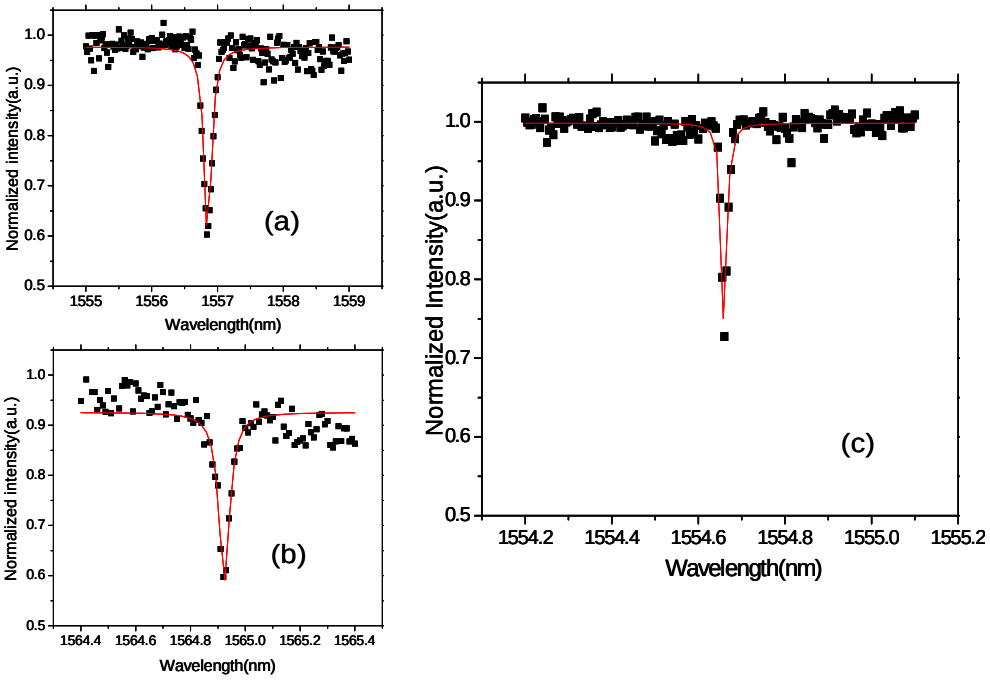

Fig. 2. Transmission spectrum of polymer micro-ring fabricated from the mold (a) without resist reflow process, (b) with resist reflow process, (c) with resist reflow and thermal oxidation process. All the black dot curves are experimental data and red line curves are Lorentz fitting curves

Figure 2(a) and 2(b) show the transmission spectrum of a polymer micro-ring imprinted using the silicon mold without and with resist reflow process, respectively. Figure 2(a) shows the total Q of around 1×10^4, and Fig. 2(b) shows the total Q of around 3×10^4. The amplitude attenuation factor can be obtained from the micro-ring transmission equation, which can be expressed as:

$$T = \frac{\tau^2 + a^2 - 2a\tau\cos\varphi}{1 + \tau^2 a^2 - 2a\tau\cos\varphi}, \tag{2}$$

#137270 - $15.00 USD Received 27 Oct 2010; revised 18 Dec 2010; accepted 23 Dec 2010; published 6 Jan 2011

where τ is the field coupling coefficient between the input and output port, a is the amplitude attenuation factor, and ϕ is the round trip phase. The amplitude attenuation is due to the various optical losses in the micro-ring, and therefore can be used to obtain the $Q_{intrinsic}$. The amplitude attenuation factor a is related to the intrinsic Q by the following equation [24]:

$$Q_{\text{int}\,rinsic} = \frac{4\pi^2 R n_{eff}}{|2\ln a|\lambda_0} \tag{3}$$

where R is the radius of the micro-ring, n_{eff} is the effective refractive index of the resonance mode and λ_0 is the resonance wavelength. By fitting with Eq. (2), we can get the field coupling coefficient between the input and output port $\tau = 0.990$ and the amplitude attenuation factor $a = 0.925$ for the micro-ring device fabricated using the mold without the resist reflow process. The calculated intrinsic Q according to Eq. (3) is around 1.2×10^4, corresponding to a propagation loss of 22.7 dB/cm. For the device created from the mold with the resist reflow process, we find that the field coupling coefficient between the input and output port $\tau = 0.996$ and the amplitude attenuation factor $a = 0.975$. The calculated intrinsic Q is around 3.5×10^4, corresponding to the propagation loss of 7.7 dB/cm. Therefore the resist reflow process can reduce the optical propagation loss by a factor of 3. Figure 2(c) shows the transmission spectrum of the waveguide coupled micro-ring devices fabricated from the mold made with the process including the resist reflow and thermal oxidation steps. The total Q is fitted to be around 1.1×10^5, and the field coupling coefficient between the input and output port is found to be $\tau = 0.99946$ while the amplitude attenuation factor is $a = 0.994$. The intrinsic Q is calculated to be~1.5×10^5, which represents propagation loss of 1.8 dB/cm. The thermal oxidation step further helps with reducing surface roughness leading to a total reduction of propagation loss by more than one order of magnitude.

COMSOL multi-physics software was used to simulate the radiation loss of the polymer micro-ring devices [25]. By taking the advantage of the axial-symmetry of the resonance modes in the micro-ring, the 3-dimensional eigenvalue problem can be transformed to an equivalent 2-dimensional problem. The exact dimensions of the micro-rings which are used in the simulation were obtained from scanning electron microscope (SEM) while the refractive index of polymer was found using spectroscopic ellipsometry. By solving the eigenvalue problem in COMSOL, we obtained the eigen frequency for the transverse electrical mode's in the micro-ring with real part equal to 1.930625×10^{14} and imagery part equal to 1.00754×10^8 Hz. Therefore the radiation loss-related $Q = \text{Re}(\omega)/2\text{Im}(\omega)$ [26] is 9.6×10^5.

To determine the absorption loss-related Q factor in the polymer micro-ring, we adopted a method based on the thermal-instability phenomenon of polymer resonators. We measured the transmission spectrum for different input powers, and the results are shown in Fig. 3. When increasing the input power, we found that the transmission spectra exhibit two notable changes: (1) the resonance peak shifts to a shorter wavelength, which is mainly due to the negative value of the opto-thermal coefficient of the polymer, and (2) distortion of resonance line shape, which is due to the material absorption induced thermal bi-stability effect [27]. The absorption loss-related Q can be extracted from the linear relation between the internal cavity energy and absorbed power by following the method described in Reference 28. Assuming steady-state condition, the absorbed power in the cavity can be expressed $P_{abs} = \Delta T/R_{th}$, where ΔT is the temperature change in the cavity, and R_{th} is the effective thermal resistance, which includes the thermal resistance of the heat sink from the polymer cavity to ambient and thermal resistance of cavity itself. This was modeled using COMSOL multi-physics and found to be 9.5×10^3 W/K. The absorbed power then can be expressed as:

$$P_{abs} = \frac{1}{\lambda\left(\alpha + \frac{1}{n}\frac{dn}{dT}\right)R_{th}}\Delta\lambda. \tag{4}$$

#137270 - $15.00 USD Received 27 Oct 2010; revised 18 Dec 2010; accepted 23 Dec 2010; published 6 Jan 2011

where n is the refractive index of the polymer, λ is the resonance wavelength, dn/dT is the thermo-optical coefficient,α is the thermal expansion coefficient and $\Delta\lambda$ is the resonance wavelength shift. Figure 4 shows the power dependence of the absorption effect from of the polymer micro-ring. The intra-cavity energy (U_c) is calculated according to the Reference 28. The linear absorption related coefficient $\gamma_{lin} = P_{abs}/U_c$ was extracted and found to be 5.6×10^9 Hz, which can be used to calculate the absorption loss-related $Q = \omega/\gamma_{lin} = 2.1 \times 10^5$ [28]. This corresponds to a material absorption loss of 1.3dB/cm for the polystyrene used in our devices, which is consistent with the published data [29].

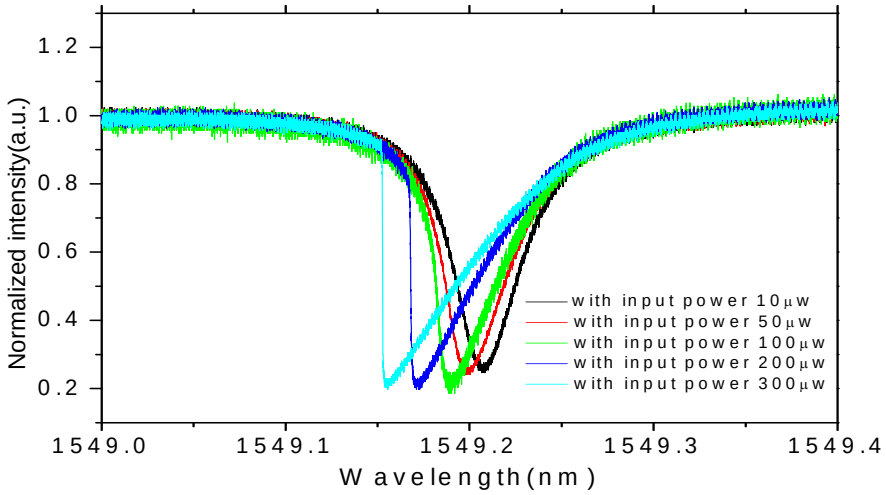

Fig. 3. Transmission spectra of polymer micro-rings with different input power.

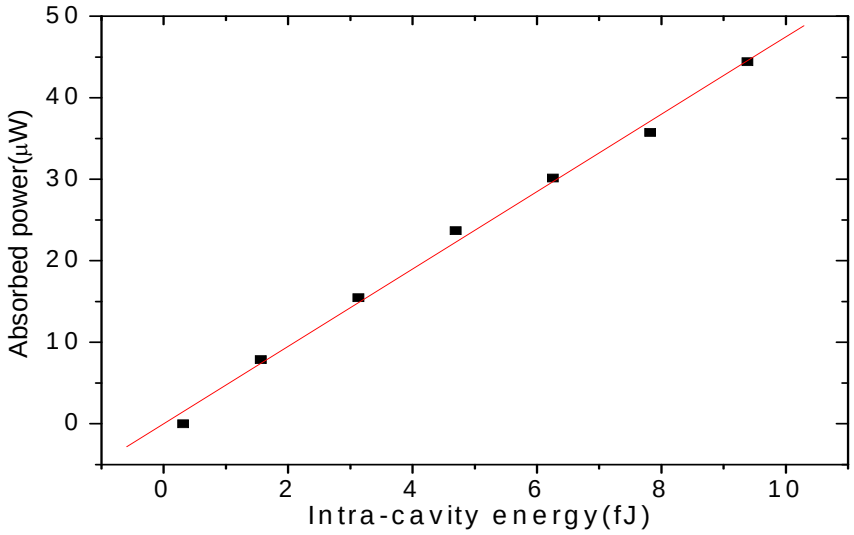

Fig. 4. Relationship between intra-cavity energy and absorbed power.

Finally, the surface scattering loss-related Q can be calculated from the Eq. (1) and is ~1.2×10^6, and the surface scattering loss can be shown as low as 0.23 dB/cm. From this analysis, we know that the dominating loss in polymer micro-rings at 1.55 μm wavelength range is the material absorption loss (~1.3dB/cm), which is attributed to the carbon-hydrogen bonds

#137270 - $15.00 USD Received 27 Oct 2010; revised 18 Dec 2010; accepted 23 Dec 2010; published 6 Jan 2011

harmonic absorption in the near-IR range. Such absorption loss can be minimized by replacing H with F atoms. Fortunately, in the visible wavelength range, polymer materials can have an absorption loss as low as 0.004dB/cm [30]. Therefore, we believe that our polymer micro-ring's total Q can be greatly increased by moving the working wavelength from the NIR to the visible range.

4. Acoustic sensitivity characterization

A 20 MHz unfocused transducer (V316, Panametrics NDT, Waltham, MA) was used to characterize the ultrasonic sensitivity of the high Q polymer micro-ring. During the experiment, the micro-ring device was immerged in de-ionized (DI) water which was used as a coupling medium for the acoustic wave. The device's transmission spectrum (Fig. 5(a)) were measured in DI water and found to have a Q factor of 2×10^4 and 93% of the optical power has been coupled into micro-ring resonators at the resonance wavelength. The intrinsic Q of the polymer micro-ring in water is fitted to be 4×10^4, which is nearly 4 times lower than that in air. This reduction of Q is mainly due to the increase in bending loss due to a reduced refractive index contrast between the waveguide core and the water cladding and absorption loss by the surrounding DI water. The transducer is driven by a 10 V peak-to-peak one cycle 20 MHz sinusoidal wave, outputting a peak pressure of 30 kPa, which was calibrated by a commercial hydrophone. The laser input was set at 1555.975 nm wavelength and the power at 5 mW. When the acoustic pressure pulse is incident on the polymer micro-ring, it modulates the resonance wavelength and therefore the output power at a fixed probing wavelength. Figure 5(b) shows the recorded signal trace from a single-shot acoustic wave. The device produces an output of 1089 mV with an input of 30 kPa acoustic pressure, which means the device's acoustic sensitivity is around 36.3 mV/kPa. This is 3.3 times larger than what we recorded previously using a device with Q of ~6000 and the same measurement system [17], including the laser, photodetecor, and oscilloscope. The root-mean-square noise levels were 1.8, 2.7, and 3.2 mV for 1–25, 1–50, and 1–75 MHz bandwidths, respectively. Thus, the corresponding NEPs are 51, 74, and 88 Pa for 1–25, 1–50, 1–75 MHz bandwidths, respectively. Therefore we have improved the NEPs nearly three times as compared with our previous best result of 230 Pa, which represents the highest sensitivity ultrasound transducer of similar physical size.

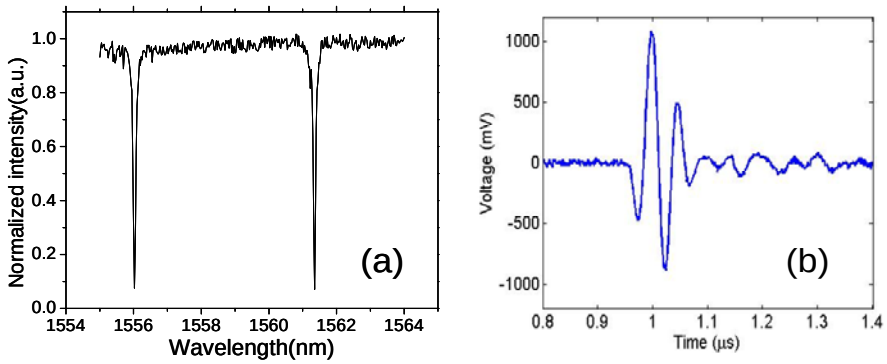

Fig. 5. (a) Transmission spectrum of polymer micro-ring immerged in DI water. (b) Single shot of acoustic waveform measured by high Q polymer micro-ring.

5. Summary

By using a new fabrication process including resist reflow and thermal oxidation processes, we have successfully fabricated a silicon mold with smooth sidewalls. The imprinted devices can achieve an intrinsic Q factor as high as 1.5×10^5, which corresponds to an optical

#137270 - $15.00 USD Received 27 Oct 2010; revised 18 Dec 2010; accepted 23 Dec 2010; published 6 Jan 2011

propagation loss of 1.8 dB/cm. Different optical loss mechanisms have been studied to obtain the two important loss parameters: absorption loss of 1.3 dB/cm and surface scattering loss of 0.23 dB/cm, respectively. By using our high Q polymer micro-rings as ultrasonic sensors, we have achieved ultrasound detection sensitivity of 36.3 mV/kPa at 240 μW operating power. Due to the increased Q factor of the polymer resonator, we have obtained 3 times lower NEP as compared with our previous work. Further reduction of the NEP is possible by making higher Q micro-rings. This can be achieved, based on our analysis, by designing the micro-rings to operate at visible optical wavelength where the absorption loss of polymer and water (used as a coupling media in ultrasound experiment) is much lower.

Acknowledgements

The authors acknowledge the support by National Institutes of Health (NIH) grant EB007619.

#137270 - $15.00 USD Received 27 Oct 2010; revised 18 Dec 2010; accepted 23 Dec 2010; published 6 Jan 2011